J. Plasma Phys. (2015), *vol.* 81, 495810503 © Cambridge University Press 2015
doi:10.1017/S0022377815000677

Low-power radio-frequency excitation as a plasma source in a Penning–Malmberg trap: a systematic study

G. Maero[1,2,†], S. Chen[3,2], R. Pozzoli[1,2] and M. Romé[1,2]

[1]Dipartimento di Fisica, Università degli Studi di Milano, Via Celoria 16, 20133 Milano, Italy

[2]INFN Sezione di Milano, Via Celoria 16, 20133 Milano, Italy

[3]Institute of Fluid Physics, China Academy of Engineering Physics, Mianyang, Sichuan 621900, China

(Received 30 April 2015; revised 20 May 2015; accepted 20 May 2015)

A novel method was experimentally demonstrated to produce a low-density electron plasma in a Penning–Malmberg trap, exploiting the static electric and magnetic confinement fields together with a periodic excitation with amplitudes as low as 0.5–5 V and frequencies in the MHz range. This unusual technique proved to be applicable as a replacement for conventional electron sources in Penning devices and presents interesting aspects both in terms of basic science and technological applications. Nevertheless, the experimental observations demonstrate the high sensitivity of plasma features of interest (charge, mean density and density distribution) to the experimental conditions, namely trap configuration and excitation parameters, and as a consequence clear trends have not been identified so far. We present an experimental campaign of measurements where several parameters were systematically changed leading to a better assessment of the plasma production mechanism and to the identification of common trends.

1. Introduction

Penning (Pierce 1949) and Penning–Malmberg (Malmberg & deGrassie 1975) traps are devices where the confinement of electrically charged particle samples with a single charge sign is made possible by the superposition of a uniform axial magnetic field and an axial electrostatic potential well (typically harmonic in Penning traps and flat-bottomed in the Penning–Malmberg variant) created by a stack of azimuthally-symmetric (cylindrical) electrodes. Together with ultra-high vacuum (UHV) conditions these characteristic features allow long-time confinement as well as precise control and manipulation of particle samples. Successful applications of traps span a wide range of research fields, from accurate measurements of fundamental properties of charged species like highly-charged ions, radioactive nuclides, antimatter (Brown & Gabrielse 1986; Blaum 2006; Block *et al.* 2006; Herfurth *et al.* 2006; Aghion *et al.* 2014; Saitoh *et al.* 2014) to collective properties of non-neutral plasmas (see e.g. Davidson 1990; Driscoll & Fine 1990; Durkin & Fajans 2000; Romé & Lepreti 2011; Lepreti *et al.* 2013) and beams (Bettega *et al.* 2004; Paroli

† Email address for correspondence: giancarlo.maero@unimi.it

https://doi.org/10.1017/S0022377815000677 Published online by Cambridge University Press

et al. 2010*a*, 2012). Ion pump technology (Audi & de Simon 1987) and chemical analysis by mass spectrometry (Amster 1996) also rely on the Penning trap concept.

In many of the aforementioned physics investigations, the common feature is the stable equilibrium of the confined sample, which then helps in the study of the free evolution or precise and repeatable manipulation of the trapped particles on the experimental side, and at the same time in a simple modelling on the theoretical side. The most obvious sources of complications are deviations from this condition. For instance, this is the case for: multispecies plasmas, i.e. samples made up by particles of different species and even opposite sign of charge, occurring in situations involving sympathetic cooling (Maero *et al.* 2012), antimatter formation (Gabrielse *et al.* 2002; Andresen *et al.* 2011), presence of transient ions (Fajans 1993) or heavy contaminants (Maero *et al.* 2014; Maggiore *et al.* 2014); non-ideal traps (Coppa, D'Angola & Mulas 2012); field fluctuations and mechanical imperfections (Kabantsev *et al.* 2014); nonlinear effects due to strong radio-frequency (RF) excitations (Huang *et al.* 1997).

We present a systematic investigation concerning the generation of an electron plasma in a Penning–Malmberg trap by means of a continuous RF excitation applied to one of the device's electrode. Experiments show that a drive of suitable frequency and amplitude in the volt range can lead to the production of electron plasma columns with total charge and density comparable to those of typical sources used by traps, such as thermo-, photo- or field-emission cathodes. Although the drive power is orders of magnitude lower than that of usual plasma production in RF discharges, the RF amplitude is comparable to the space charge potential of the plasma. Furthermore, since the basic mechanism of plasma production is the ionization of the residual gas, ions are always present in the trapping volume and may give rise to well-known instability effects (Fajans 1993; Bettega *et al.* 2005), and changes in the control parameters lead to the production of plasmas with extremely different characteristics. Despite the difficulties in the interpretation of experimental observations, previous experiments have demonstrated several interesting features of the RF-generated plasma and secondary phenomena concerning its stability properties (Paroli *et al.* 2010*b*, 2014). The goal of the experimental campaign we discuss in the following is to gain a better understanding of the plasma generation as a function of the control parameters, so as to possibly identify optimal conditions and to suggest key features leading to a thorough modelling of this system.

In the next section we briefly present the apparatus and detail the procedure used in the RF plasma generation. We report on the experimental observation of the general features of plasmas obtained with this technique. The routine followed in all subsequent systematic experiments is discussed and the issue of repeatability is assessed. Section 3 is devoted to systematic experiments where we compare the results obtained upon the variation of a selection of control parameters. In § 4 we summarize the main results and draw our conclusions on the points of interest raised by the current observations, concluding with an outline of future experimental and theoretical works that may help to address the questions left open.

2. Generation mechanism: experimental routine and repeatability

2.1. *Set-up and main features of RF-generated plasmas*

The experiments presented here were performed in the ELTRAP (ELectron TRAP) Penning–Malmberg device, a machine where a vacuum vessel kept in the UHV regime (typically 10^{-8}–10^{-9} mbar) houses a stack of 12 cylindrical electrodes (sketched in

https://doi.org/10.1017/S0022377815000677 Published online by Cambridge University Press

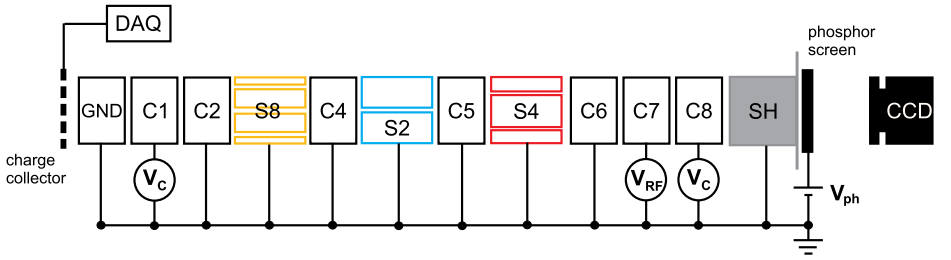


FIGURE 1. Sketch of the trap electrode arrangement. Outer electrodes GND and SH are permanently grounded. Any pair of two electrodes can be set to a confinement potential V_C to be used as endcaps while another one is employed as excitation antenna with an oscillating voltage signal V_{RF}. Diagnostic tools are also sketched: a charge collector connected to a high-impedance digital oscilloscope and a phosphor screen set to a potential $V_{ph} = 5$–15 kV, whose image is recorded by a CCD camera.

figure 1) with a maximum trapping length L_{trap} of about 1 m and a 45 mm radius R_W. While the two outermost electrodes are permanently grounded to ensure a well-defined potential outside the trapping region, any pair of inner electrodes can be used as endcaps to create a positive or negative well with a depth $V_C \leqslant 100$ V. The vessel is surrounded by a solenoid providing a highly homogeneous axial magnetic field $B \leqslant 0.2$ T. In these conditions, typical low-temperature electron plasmas are highly magnetized, with a cyclotron frequency $\nu_c = eB/2\pi m$ (where e and m are the electron charge and mass) in the GHz range and a cyclotron radius orders of magnitude smaller than R_W. Other typical frequencies, characteristic of the transverse $\boldsymbol{E} \times \boldsymbol{B}$ drift, are the plasma rotation frequency ν_r and the frequencies of diocotron (azimuthal) l-modes ν_l that lie in the 10–100 kHz range. The axial bounce frequency ν_z is about 0.1–1 MHz for temperatures of few eV. These motions are therefore decoupled in the non-collisional regime, yet collisions may become relevant in long-time experiments, as the electron–electron collision frequencies have values around some 100 Hz and electron–neutral collision frequencies lie in the 1–10 Hz range. Non-destructive diagnosis of the plasma transverse motion is possible by monitoring the current induced by the plasma itself on azimuthally split electrodes S2, S4, S8 (segmented into two, four and eight equal patches, respectively). Grounding one of the endcaps allows the plasma to flow out and to be intercepted either by a collector plate or by a phosphor screen biased at a positive voltage $V_{ph} \sim 5$–15 kV, respectively, so that the total charge or the axially-integrated electron distribution is acquired.

Contrary to customary Penning traps exploiting electron sources like thermocathodes or photocathodes, the RF production mechanism discussed here is 'sourceless' in that it uses no additional physical apparatus. The procedure starts with a confinement configuration where two endcaps are biased to a negative potential $V_C = 80$–100 V and all other electrodes are grounded apart from a chosen electrode within the confinement region, set at a sinusoidally varying voltage $V_{RF} \sin(2\pi\nu_{RF}t)$ with a typical amplitude $V_{RF} = 1$–5 V and a frequency ν_{RF} ranging from 1 to some 10 MHz. An electron plasma can be detected in times of the order of some 100 ms and a stable distribution characterized by a dynamical equilibrium between continuous formation and losses is reached after some seconds. In particular, axial losses of electrons with an energy overcoming the trapping barrier can be detected in the form of continuous currents up to some nA flowing onto the collector. Even if ions are not effectively confined, ionization must also produce a continuous flux of molecular

https://doi.org/10.1017/S0022377815000677 Published online by Cambridge University Press

ions through the trapping volume. So far, we have not been able to obtain any direct information on the ion plasma component, whose measurement presents technical difficulties. In other experiments *ad hoc* diagnostic techniques have been developed to this end (Kabantsev & Driscoll 2004) which are not easily applied in our system.

A qualitative explanation of the plasma generation phenomenon can be given on the basis of simple arguments. Given the axisymmetric geometry of the confinement and excitation electrodes and the frequency range of the RF drive, free electrons in the background gas may be heated, predominantly in the axial direction, which in turn may lead to ionization of the residual gas when the electrons reach sufficient kinetic energy, following a mechanism of stochastic nature (Lichtenberg & Lieberman 1983). An interpretation of heating and ionization phenomena in terms of stochastic heating due to oscillating electric fields has been proposed in the past, e.g. in the context of RF discharges at higher pressures (10^{-3}–1 mbar) where extended experimental results as well as theoretical models have been obtained (Lieberman & Godyak 1998; Wang, Lichtenberg & Cohen 2012). In our experimental observations typical plasma formation times (hundreds of ms) match the aforementioned collisional times and the RF drive frequencies agree with the bounce frequencies of electrons with axial kinetic energy of few to tens of eV, thus qualitatively confirming this interpretation. Further details can be found in Paroli *et al.* (2010*b*) and Romé *et al.* (2015). Linear and nonlinear resonances of the RF field with the axial particle motion or with longitudinal collective modes can also contribute to the heating effect.

Over the course of many experiments we observed that additional ionization sources, e.g. UV rays or static high voltages (HV), may help to initiate the discharge. This is particularly helpful at the beginning of the experiment, i.e. UV or HV can be used as an initial trigger when starting from scratch and then switched off so that the subsequent generation of further electron samples after ejection of the previous, early plasmas can continue without additional help. Please note that in order to use the optical diagnostics we necessarily set the phosphor screen to a voltage in the kV range. In order to avoid possible distortion in the results, the phosphor voltage has been permanently switched on at a value of 8 kV for all experiments presented in the following. Nevertheless it is important to remark that many experiments have been performed where we could attain repeated 'create–hold and measure–dump' sequences of RF-generated plasmas without the need for UV or HV; therefore we can exclude the possibility that these represent the direct origin of the observed phenomena.

Plasmas generated by means of this procedure reach a total charge up to about 1 nC and particle densities in the range 10^6–10^7 cm^{-3}. The plasma is most frequently produced close to the electrode surface in the early formation stage over typical time periods in the 100 ms range. The charge progressively builds up and may reach a status where it covers the whole trap cross-section. As we will see in the following, in general the density is relatively low with respect to specific events that we could observe, namely the formation of columns with a narrower mean radius R_p or the transition from a diffuse plasma to a denser and smaller cross-section. These electron plasmas can have a radius as small as $R_p/R_W \leqslant 0.1$ and yield particle densities above 10^7 cm^{-3}, and we have previously exploited this phenomenon mainly as a substitute for a more conventional electron plasma source, as it allows us to 'prepare' an electron column for the following observation stage where the excitation drive is switched off and the plasma is left free to evolve. In such cases the RF generation phenomenon is used as a tool and we empirically adjust the control parameters in order to achieve a plasma with the desired features to perform a subsequent experiment.

The narrow-radius plasmas exhibit further interesting features. They are often produced at a radial offset with respect to the magnetic axis and hence exhibit

https://doi.org/10.1017/S0022377815000677 Published online by Cambridge University Press

an $l = 1$ diocotron mode (i.e. a drift around the magnetic axis). Experiments on quiescent plasma columns have shown that the $l = 1$ mode is unstable in the presence of various sources of dissipation, including the presence of positive ions (Fajans 1993). Continuous ionization implies the presence of ionic species in the trap during the RF plasma generation; we found that as long as the RF drive is on, the mode is stable or presents a slow amplitude and frequency modulation (Paroli *et al.* 2014).

All experiments presented in the following were performed according to a common routine, namely the repetition of the 'create–hold–dump' loop and the acquisition of the image formed on the phosphor screen at the release of the plasma and recorded by a charge-coupled device (CCD) camera with a maximum resolution of 1344 pixel × 1024 pixel. Each 5 s loop consisted of a confinement time of 4.5 s with trapping potentials of −80 V followed by a 0.5 s stage with grounded endcap on the phosphor side, thus allowing the ejection of the plasma and ensuring that the trap was empty at the start of the following cycle. A transistor–transistor logic (TTL) signal synchronized with the plasma ejection triggered the CCD image acquisition. The CCD intensity level, cleaned from the background noise, was previously calibrated in order to yield the corresponding density distribution. The calibration was performed by comparing the sum of all pixel intensities of the CCD image produced by a set plasma with the plasma's total charge. This value can be calculated if the same plasma is dumped on the collector placed at the opposite trap end. The peak voltage of the resistor–capacitor (RC) discharge measured on the oscilloscope yields the charge deposited on the collector once the network's parasitic capacitance has been calculated from the exponential slope of the discharge. In each single run we fixed a common set of control parameters, namely the RF amplitude, the trap length and the magnetic field strength. In order to do a faster, automated data acquisition, instead of manually setting a fixed RF frequency for each cycle, ν_{RF} was continuously swept in the range 0.1–10 MHz with a sweep rate of 20 kHz s^{-1}, corresponding to a variation of 90 kHz during a 4.5 s confinement cycle and equivalent to the acquisition of 100 data points over a total sweep time of 500 s. Some experiments (mentioned in the following) were performed doubling the resolution, yielding 200 data points in the range 0.05–10 MHz, and showed a perfect agreement with those at lower resolution. In the systematic investigations presented in the next sections, this routine was repeated, varying each time the value of a single control parameter.

The electrode chosen as antenna for the RF drive was always the closest to one of the endcaps, i.e. electrode C7 as we always used C8 as an endcap (eventually varying the other endcap during the trapping length parametric study discussed in § 3.1). This defines two axial trapping regions (with respect to three regions if one of the innermost electrodes is chosen), providing the simplest configuration. Furthermore, as the 90 mm long C7 cylinder has no azimuthal splitting, in principle no transfer of angular momentum is involved in the excitation (unless magnetic field tilts or other mechanical/electrical imperfections are present).

An example of the results obtained with the frequency-sweep looped measurement is summarized in figure 2. Figure 2(*a*) reports the total confined electron charge obtained as the sum of the pixel intensities of the CCD image after de-noising and intensity calibration. Figure 2(*b*) reports an approximate estimate of the corresponding mean electron density. This is calculated as the average density over the area of the image whose intensity is larger than half of the peak value. This may be a rather crude approximation for plasmas featuring low densities and irregular cross-sections, yet it allows us to recognize at a glance and unambiguously density peaks and to evaluate their core density. Some typical examples of plasmas that may be produced

https://doi.org/10.1017/S0022377815000677 Published online by Cambridge University Press

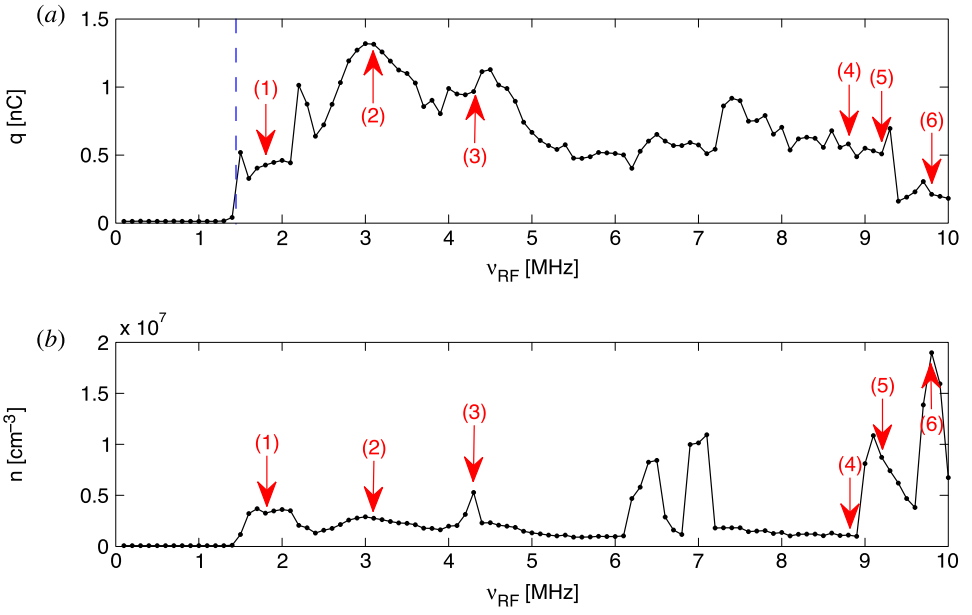


FIGURE 2. Example of frequency sweep measurement. Trap length $L_{trap} = 570$ mm, magnetic field $B = 0.1$ T, excitation amplitude $V_{RF} = 1.5$ V. (*a*) Total confined electron charge. The vertical dashed line indicates the threshold frequency ν_{thr} for plasma production and confinement. (*b*) Mean particle density. The transverse distributions of plasma corresponding to data points indicated by red arrows are plotted in figure 3.

with the RF technique are indicated by red arrows and their corresponding CCD images are plotted in figure 3, where we can see: diffuse plasmas; narrow-radius columns, which are often surrounded by a lower-density background (case 3) or even halo rings (case 6) when they reach the highest attained densities (some 10^7 cm^{-3}); quadrupole deformations (case 5).

The diagrams in figure 2 also show another prominent feature of the RF plasma production, i.e. the existence of a distinct frequency threshold ν_{thr} beyond which the confined electron charge can be observed. This threshold is always present and we will investigate it further in the following, and we define ν_{thr} as the frequency corresponding to half of the charge level measured right after the first detectable rise in the charge versus frequency pattern.

2.2. *Repeatability of RF-generated plasmas*

Given the nature of the plasma generation process it is clear that the results will be extremely sensitive to the experimental conditions. Therefore the reproducibility of results must be assessed before any further data analysis and interpretation can be performed. We have partially addressed this issue in past experiments where repeated measurements had to be performed by means of a looped 'create–hold and measure–dump' procedure. This routine is typical of our experiments on low-order diocotron (Kelvin–Helmholtz) instabilities, for which we use a circular plasma column with a narrow radius and relatively high density ($n \simeq 10^7$ cm^{-3}). In these cases we estimate that once the desired plasma is achieved and the set of parameters is fixed, the variations in the charge distribution at several successive plasma dumps are

https://doi.org/10.1017/S0022377815000677 Published online by Cambridge University Press

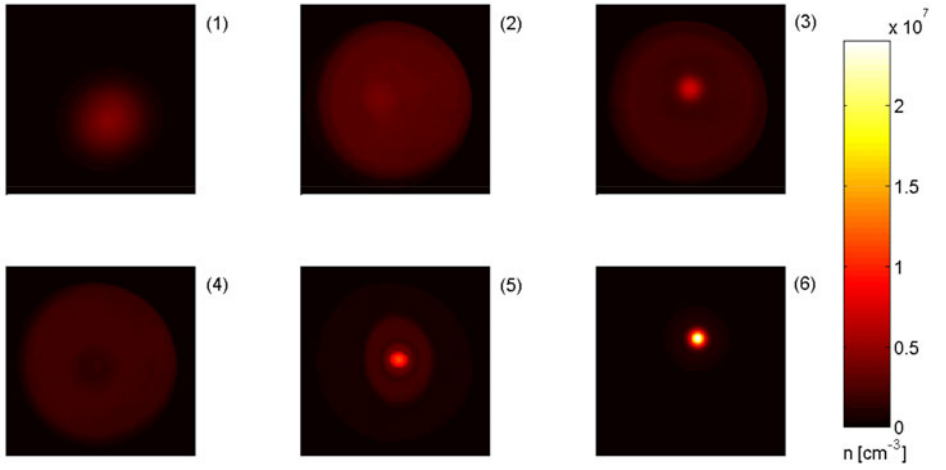


FIGURE 3. Examples of RF-generated electron plasmas. The axially-integrated transverse distributions of some of the plasmas from figure 2 are visualized as de-noised CCD images at plasma dump. Images numbered from 1 to 6 correspond to the frequencies 1.8, 3.1, 4.3, 8.8, 9.2 and 9.8 MHz, respectively (also indicated in figure 2).

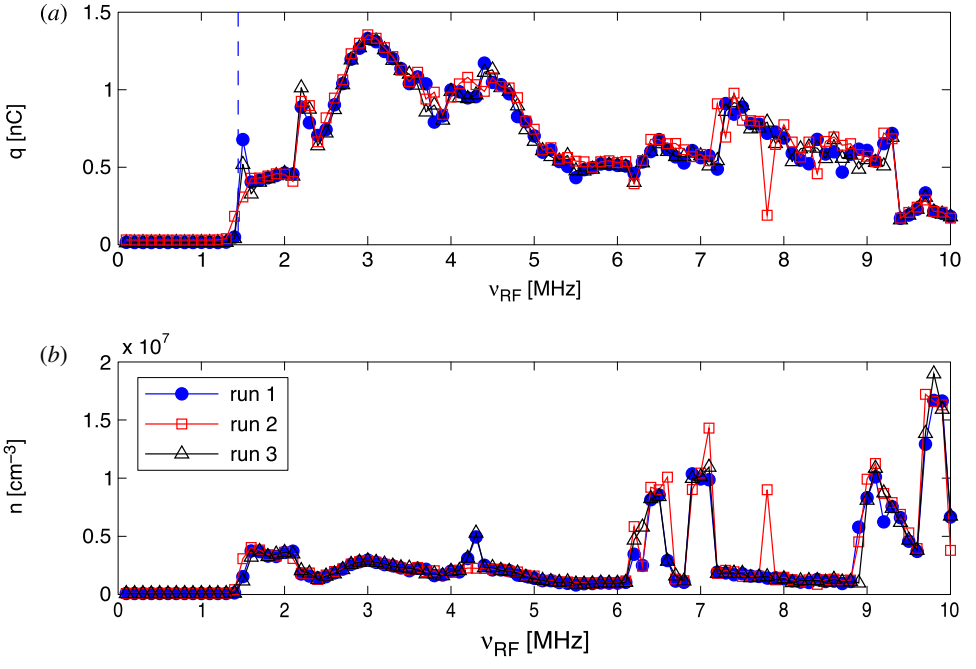


FIGURE 4. Repeatability test. The three frequency scan measurements were recorded during a single experiment/day with the same set of parameters, i.e. trapping length $L_{trap} = 570$ mm, magnetic field $B = 0.1$ T, excitation amplitude $V_{RF} = 1.5$ V. (*a*) Total confined charge. The vertical dashed line indicates the threshold frequency ν_{thr} for plasma production and confinement. (*b*) Mean particle density.

https://doi.org/10.1017/S0022377815000677 Published online by Cambridge University Press

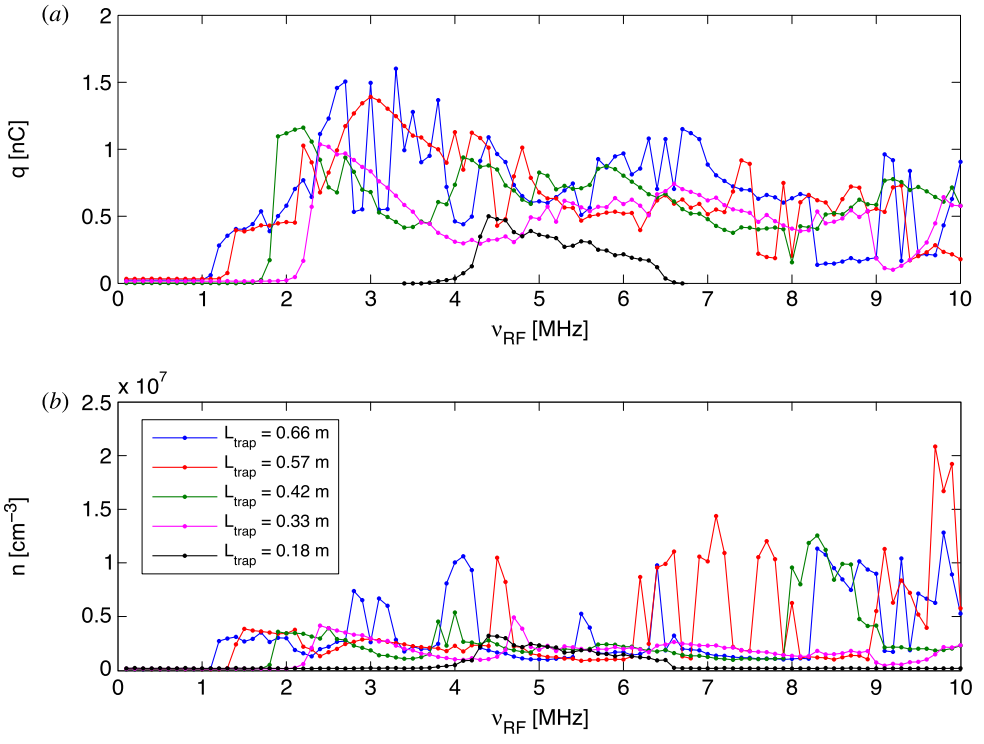


FIGURE 5. Parametric measurement of plasma production against trapping length. (*a*) Total confined electron charge. The electron plasma produced by RF excitation is measured while slowly sweeping the RF frequency ν_{RF} at constant amplitude $V_{RF} = 1.5$ V and magnetic field $B = 0.1$ T. The measurement is repeated for different axial trap lengths. (*b*) The corresponding mean electron density is plotted.

below few per cent if the experimental conditions are stable. Plasmas with different characteristics can still be randomly generated, but their occurrence is quite infrequent and they can easily be recognized by means of electrostatic or optical diagnostics and thus discarded (Maero *et al.* 2011).

In the current experimental campaign, when repeating frequency scans at constant parameters the total charge trends are also fairly well reproduced over the course of a single experiment, typically spanning one day at most. As an example we may look at figure 4, showing three runs with excitation amplitude $V_{RF} = 1.5$ V in a 570 mm long trap and magnetic field $B = 0.1$ T. An estimate of the accuracy can be obtained by looking at the most prominent shapes in the curves, e.g. the first rise in total charge at the lower frequency threshold. This feature, as well as other recognizable patterns, may exhibit a horizontal (frequency) fluctuation of around ± 50 kHz, i.e. of about one data point. The vertical (total charge) fluctuation in these qualitatively repeatable patterns is of the order of 10 %.

More significantly, further deviations occur where single data points scatter widely from otherwise similar patterns. These events can be related to two different reasons: (*a*) the formation of a narrow, high-density plasma column; (*b*) the occasional presence of low-frequency (LF) modulation of the $m = 1$ diocotron mode in a narrow column. The transition from a diffuse plasma to a narrow column is a complicated phenomenon whose discussion is left to a separate paper; for now, we simply remark that we have

https://doi.org/10.1017/S0022377815000677 Published online by Cambridge University Press

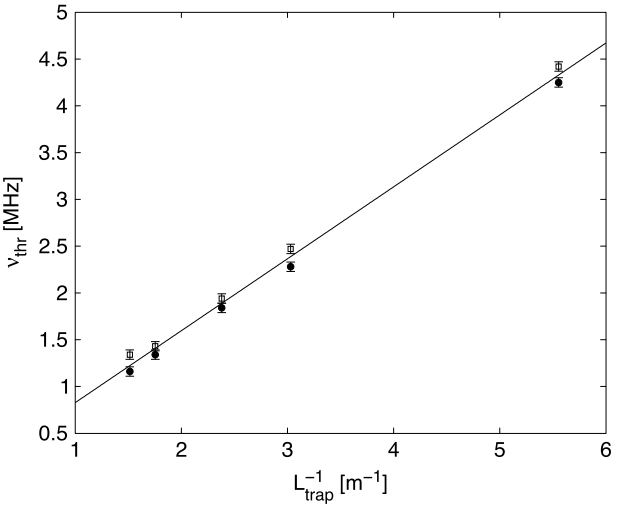


FIGURE 6. Threshold frequency versus the inverse of the trapping length. Two data sets (solid circles and hollow squares) from two distinct experiments are shown spanning trapping lengths $L_{trap} = 180$–660 mm. All experiments were performed at constant amplitude $V_{RF} = 1.5$ V and magnetic field $B = 0.1$ T. Error bars (± 50 kHz) indicate the uncertainty of the threshold value in a single frequency sweep (as estimated in § 2.2). The solid line is a linear fit to all data.

experimentally observed that this transition is not completely deterministic, i.e. it may require a varying amount of time to occur and also may not occur at all or shift to a slightly different frequency, probably depending on fluctuations of parameters beyond our control, namely the vacuum level or the ambient temperature. An example is the density peak at 7.8 MHz visible in figure 4, which is observed for one run only (red hollow squares). The LF modulation is a phenomenon observed in a previous paper (Paroli *et al.* 2014) that is also accompanied by an oscillation of the electron column total charge and whose random initial phase results in a different charge detected over multiple measurements.

Measurements taken from different experiments/days may suffer from additional deviations (roughly of the same type and magnitude) due to the modification of experimental conditions, such as base pressure and temperature, which are subject to daily fluctuations depending on the environmental conditions and their feedback on the heat exchange in the magnet cooling system.

3. Parametric measurements

3.1. *Trap length scan*

We performed two separate experiments, each consisting of repeated RF frequency sweeps with different electrode pairs as trap endcaps, yielding trapping lengths equal to 180, 330, 420, 570 and 660 mm. All measurements were taken for a magnetic field of 0.1 T and an RF amplitude of 1.5 V, scanning the 0.1–10 MHz interval at a sweep rate of 20 kHz s^{-1} (100 data points/sweep). Diagrams reporting the total charge and mean density for one of such sets are shown in figure 5 and indicate that the threshold frequency is progressively reduced as the trap length is increased. In particular, figure 6 shows that ν_{thr} scales with the inverse of the trapping length in

https://doi.org/10.1017/S0022377815000677 Published online by Cambridge University Press

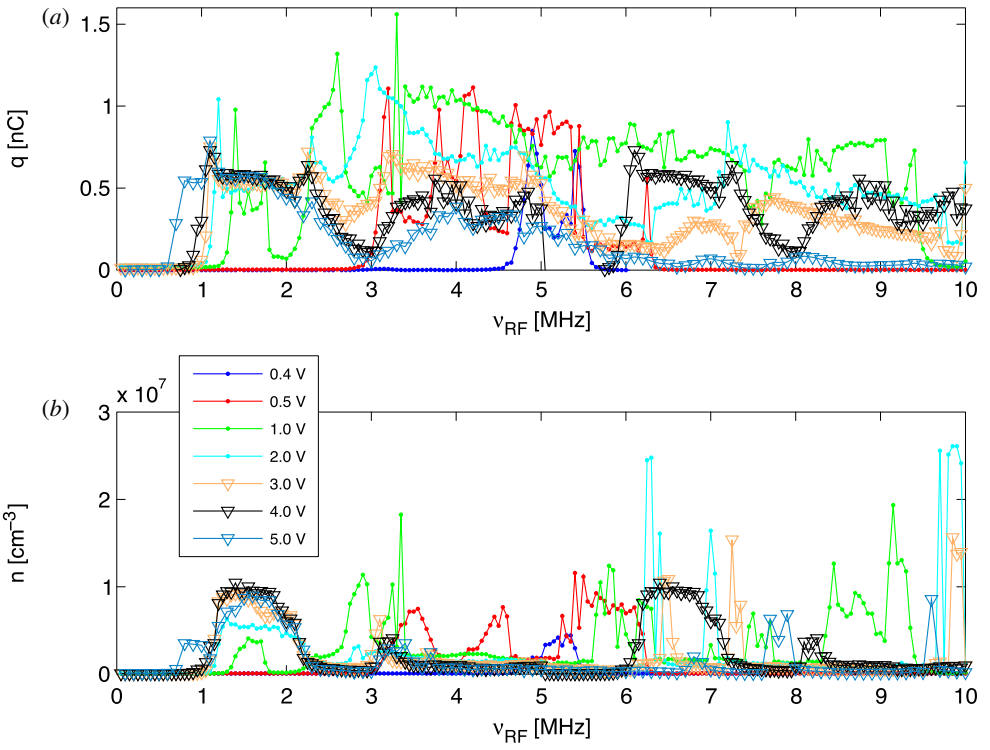


FIGURE 7. Parametric measurement of plasma production against the excitation amplitude. (*a*) Total confined electron charge. The electron plasma produced by RF excitation is measured while slowly sweeping the RF frequency ν_{RF} at constant trap length $L_{trap} =$ 570 mm and magnetic field $B = 0.1$ T. The measurement is repeated for different excitation amplitudes V_{RF}. (*b*) The corresponding mean electron density is plotted.

the measurable range. This is reasonable as it is also the scaling of the axial bounce frequency in a flat-bottomed potential well. The energy of an electron oscillating with a bounce frequency equal to that of the threshold RF drive would be approximately 7 eV.

The total confined charge increases with the trapping length, which is reasonable as the capacity of the trap increases linearly. Indeed, the charge per unit length (linear charge density) yields similar values for all cases, with the exception of the shortest trap length, where the generation is less efficient and the frequency range where plasma is detected is strongly reduced (roughly 4–6.5 MHz). In this regard one should notice that for a very short length the approximation of a flat-bottomed longitudinal well and one-dimensional axial excitation becomes inappropriate. Increasing the trap length also increases the probability of observing high-density, narrow-radius plasmas.

3.2. *RF amplitude scan*

The excitation amplitude is an obvious parameter of choice, as it can be expected to have a strong qualitative and quantitative influence on the plasma generation. Figures 7 and 8 summarize the main results obtained from three different experiments covering the amplitude range 0–5 V. One of the experiments (solid red triangles in figure 8) was conducted at the usual resolution (sweep rate 20 kHz s^{-1}, 100 data points) while

https://doi.org/10.1017/S0022377815000677 Published online by Cambridge University Press

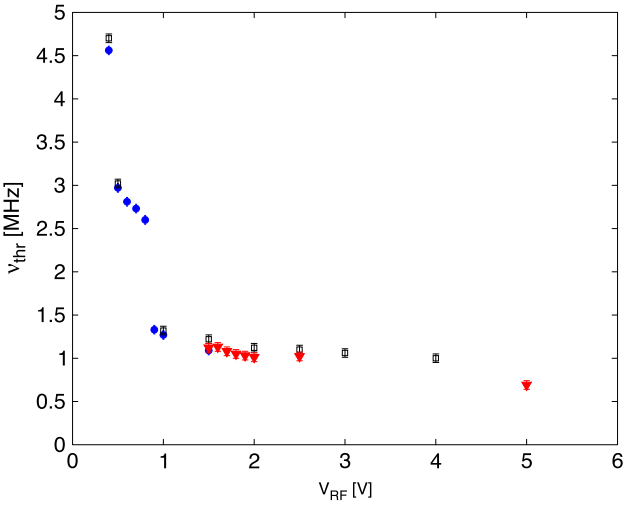


FIGURE 8. Threshold frequency versus the excitation amplitude. Data from three separate experiments (hollow black squares, solid blue circles, solid red triangles) are shown. All experiments were performed at constant trap length $L_{trap} = 570$ mm and magnetic field $B = 0.1$ T, changing the excitation amplitude V_{RF} only. Error bars (±50 kHz) indicate the uncertainty of the threshold value in a single frequency sweep (as estimated in § 2.2).

the resolution was doubled (sweep rate 10 kHz s^{-1}, 200 data points) in the other two (hollow black squares, solid blue circles in figure 8). All experiments covered the excitation frequency range $\nu_{RF} = 0$–10 MHz and were performed at constant trapping length $L_{trap} = 570$ mm and magnetic field $B = 0.15$ T.

Measurements show that electron plasmas can be detected using excitation amplitudes as low as 0.4 V and that the frequency threshold is reduced as V_{RF} is increased. Looking at figure 8, where the dependence of the lower frequency threshold on V_{RF} is plotted, one can notice that this trend is apparently not a continuous curve but rather a piecewise relation that tends to saturate at relatively large amplitudes.

In the same way, a larger V_{RF} does not correspond to a systematic increase of the produced charge; on the contrary, with the saturation of ν_{thr} at large RF amplitudes the overall trend of the total confined charge shows comparable or even smaller values. A possible explanation may be related to the fact that higher amplitudes can lead to larger electron heating and in turn to increased axial losses.

3.3. *Magnetic field strength scan*

The dependence of the plasma generation on the strength of the axial magnetic field was also investigated. Figure 9 reports the confined electron charge and density measured in a 570 mm long trap and 1.5 V excitation for magnetic fields spanning the range 0.06–0.16 T. While the increase of B has the effect of lowering the frequency threshold, it can be noticed that the overall charge versus frequency trend is largely unaffected in the ν_{RF} range above 3.5 MHz if we exclude the high-density peaks. On the contrary, the occurrence of such peaks is modified by the change of magnetic field intensity, although clear trends are not recognized.

Concerning the decrease of ν_{thr} for increasing magnetic field strength, one can observe that diffusion rates scaling with B^{-2} can be expected in magnetized

https://doi.org/10.1017/S0022377815000677 Published online by Cambridge University Press

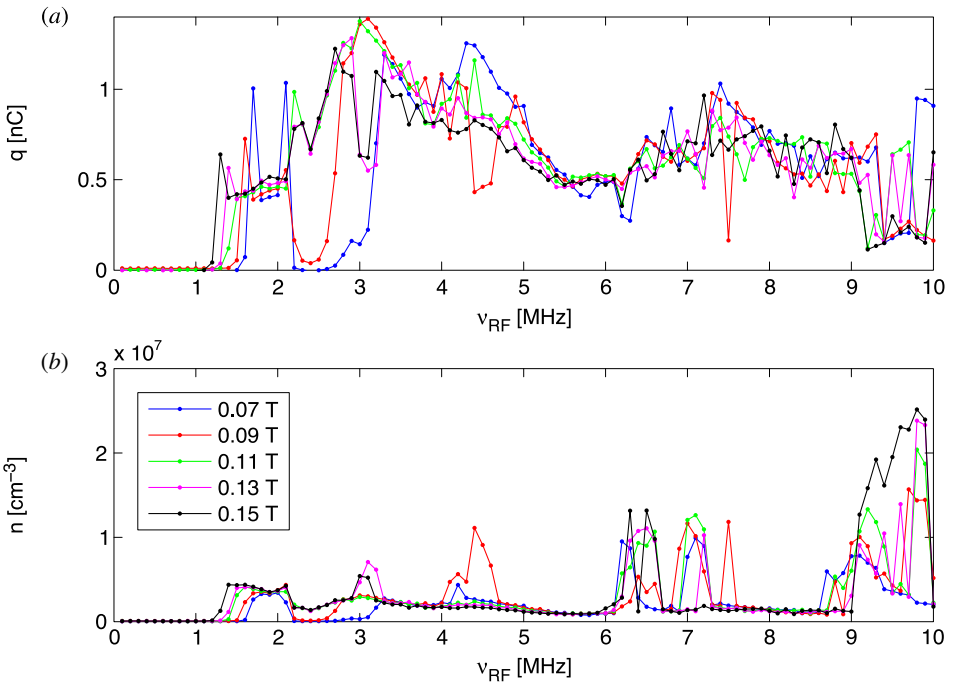


FIGURE 9. Parametric measurement of plasma production against the magnetic field intensity. (*a*) Total confined electron charge. The electron plasma produced by RF excitation is measured while slowly sweeping the RF frequency ν_{RF} at constant excitation amplitude $V_{RF} = 1.5$ V and trap length $L_{trap} = 570$ mm. The measurement is repeated for different magnetic fields. (*b*) The corresponding mean electron density is plotted.

plasmas, and confinement times scaling with B^2 in trapped non-neutral plasmas were experimentally measured (Driscoll, Fine & Malmberg 1986; Fajans 1999). The interpretation of ν_{thr} as an index of the balance between ionization and losses, leading in turn to a long-time effective confinement of the produced charge, supports the possibility of a similar scaling law. The measured threshold frequency is plotted in figure 10 against B^{-2} along with a linear fit that shows that our data are consistent with the $\nu_{thr} \sim B^{-2}$ trend.

4. Conclusions

We have performed an experimental characterization of an RF-excitation-based electron plasma production method which can be efficiently exploited in a Penning–Malmberg device. An advantage of this technique is the absence of a physical source apparatus, which may be interesting when an axial optical access is required for other experimental purposes. The possibility to ionize a gas in the UHV regime may also be relevant to technological applications like sputter-ion pumps. Systematic measurements show that plasmas with charge and density comparable to conventional electron sources can be attained within a wide range of experimentally accessible control parameters. The repeatability of this production mechanism has been assessed and some clear features have been demonstrated, namely the existence of a sharp lower frequency threshold. Both the typical excitation frequency range and inverse dependence of the threshold on the trapping length within our accessible length range

https://doi.org/10.1017/S0022377815000677 Published online by Cambridge University Press

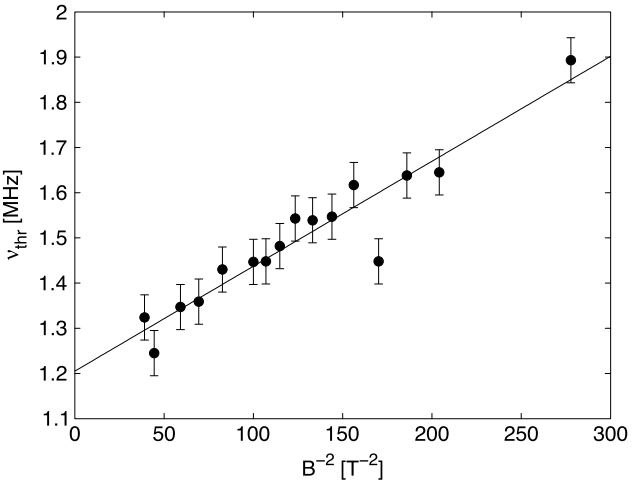


FIGURE 10. Threshold frequency dependence on the magnetic field intensity B. All experiments were performed at constant excitation amplitude $V_{RF} = 1.5$ V and trap length $L_{trap} = 570$ mm and the magnetic field was varied in the range 0.06–0.16 T. The threshold frequency ν_{thr} is plotted against B^{-2} together with a linear fit (solid line). Error bars (±50 kHz) indicate the uncertainty of the threshold value in a single frequency sweep (as estimated in § 2.2).

confirm that the electron heating leading to gas ionization takes place primarily in the axial direction, at least while the length-to-radius aspect ratio is large. The RF amplitude required to produce a detectable plasma can be as low as some 100 mV. The increase in amplitude widens the usable frequency range, reducing the threshold frequency, but this effect quickly saturates and large excitation amplitudes may result in lower confined charge, possibly because of increased electron heating and losses. The effect of the magnetic field strength, although less pronounced due to the limited range accessible in our apparatus, is a reduction of the threshold frequency with increasing magnetic field, consistent with a B^{-2} scaling.

A complete understanding of the electron plasma generation and of secondary phenomena such as high-density column formation, the presence of $l = 1, 2$ diocotron modes and their modulation is still missing. Further experimental investigations are planned in order to acquire essential information for the formulation of a theoretical model, e.g. by extending the range of the control parameters, detecting hitherto unaccessed quantities such as the ion current and possibly the electron plasma temperature, and investigating the early stage of plasma formation (0.1–1 s).

Acknowledgement

This work is partially supported by the INFN Group V within the 'COOLBEAM' project.

REFERENCES

AGHION, S., AHLEN, O., AMSLER, C., ARIGA, A., ARIGA, T., BELOV, A. S., BERGGREN, K., BONOMI, G., BRAUNIG, P., BRUSA, R. S., CABARET, L., CANALI, C., CARAVITA, R., CASTELLI, F., CERCHIARI, G., CIALDI, S., COMPARAT, D., CONSOLATI, G., DERKING, H., DI DOMIZIO, S., DI NOTO, L., DOSER, M., DUDAREV, A., EREDITATO, A., FERRAGUT,

https://doi.org/10.1017/S0022377815000677 Published online by Cambridge University Press

R., Fontana, A., Genova, P., Giammarchi, M., Gligorova, A., Gninenko, S. N., Haider, S., Huse, T., Jordan, E., Jorgensen, L. V., Kaltenbacher, T., Kawada, J., Kellerbauer, A., Lagomarsino, V., Lehner, S., Magnani, A., Malbrunot, C., Mariazzi, S., Matveev, V. A., Moia, F., Nebbia, G., Nedelec, P., Oberthaler, M. K., Pacifico, N., Petracek, V., Pistillo, C., Prelz, F., Prevedelli, M., Regenfus, C., Riccardi, C., Rohne, O., Rotondi, A., Sandaker, H., Scampoli, P., Storey, J., Vasquez, M. A. S., Spacek, M., Testera, G., Vaccarone, R., Widmann, E., Zavatarelli, S. & Zmeskal, J. 2014 A moiré deflectometer for antimatter. *Nat. Commun.* **5**, 1–6.

Amster, I. J. 1996 Fourier transform mass spectrometry. *J. Mass Spectrom.* **31**, 1325–1337.

Andresen, G. B., Ashkezari, M. D., Baquero-Ruiz, M., Bertsche, W., Bowe, P. D., Butler, E., Cesar, C. L., Charlton, M., Deller, A., Eriksson, S., Fajans, J., Friesen, T., Fujiwara, M. C., Gill, D. R., Gutierrez, A., Hangst, J. S., Hardy, W. N., Hayano, R. S., Hayden, M. E., Humpries, A. J., Hydomako, R., Jonsell, S., Kemp, S. L., Kurchaninov, L., Madsen, N., Menary, S., Nolan, P., Olchanski, K., Olin, A., Pusa, A., Rasmussen, C. O., Robicheaux, F., Sarid, E., Silveira, D. M., So, C., Storey, J. W., Thomson, R. I., van der Werf, D. P., Wurtele, J. S. & Yamazaki, Y. 2011 Confinement of antihydrogen for 1000 s. *Nat. Phys.* **7**, 558–564.

Audi, M. & de Simon, M. 1987 Ion pumps. *Vacuum* **37**, 629–636.

Bettega, G., Cavaliere, F., Cavenago, M., Illiberi, A., Pozzoli, R. & Romé, M. 2005 Experimental investigation of the ion resonance instability in a trapped electron plasma. *Plasma Phys. Control. Fusion* **47**, 1697–1708.

Bettega, G., Cavaliere, F., Illiberi, A., Pozzoli, R., Romé, M., Cavenago, M. & Tsidulko, Yu. 2004 Experimental investigation of coherent structures in a low-energy electron beam. *Appl. Phys. Lett.* **84**, 3807–3809.

Blaum, K. 2006 High-accuracy mass spectrometry with stored ions. *Phys. Rep.* **425**, 1–78.

Block, M., Ackermann, D., Blaum, K., Chaudhuri, A., Di, Z., Eliseev, S., Ferrer, R., Habs, D., Herfurth, F., Hessberger, F. P., Hofmann, S., Kluge, H.-J., Maero, G., Martín, A., Marx, G., Mazzocco, M., Mukherjee, M., Neumayr, J. B., Plass, W. R., Quint, W., Rahaman, S., Rauth, C., Rodriguez, D., Scheidenberger, C., Schweikhard, L., Thirolf, P. G., Vorobjev, G. & Weber, C. 2006 Mass measurements in the endpoint region of the rp-process at SHIPTRAP. *Hyperfine Interact.* **173**, 133–142.

Brown, L. S. & Gabrielse, G. 1986 Geonium theory: physics of a single electron or ion a Penning trap. *Rev. Mod. Phys.* **58**, 233–311.

Coppa, G. G. M., D'Angola, A. & Mulas, R. 2012 Analysis of electron dynamics in non-ideal Penning traps. *Phys. Plasmas* **19**, 062507.

Davidson, R. C. 1990 *An Introduction to the Physics of Nonneutral Plasmas*. Addison-Wesley.

Driscoll, C. F. & Fine, K. S. 1990 Experiments on vortex dynamics in pure electron plasmas. *Phys. Fluids* B **2**, 1359–1366.

Driscoll, C. F., Fine, K. S. & Malmberg, J. H. 1986 Reduction of radial losses in a pure electron plasma. *Phys. Fluids* **29**, 2015–2017.

Durkin, D. & Fajans, J. 2000 Experiments on two-dimensional vortex patterns. *Phys. Fluids* **12** (2), 289–293.

Fajans, J. 1993 Transient ion resonance instability. *Phys. Fluids* B **5** (9), 3127–3135.

Fajans, J. 1999 Lifetime scaling in non-neutral plasmas. *Commun. Mod. Phys.* **1**, 123.

Gabrielse, G., Bowden, N. S., Oxley, P., Speck, A., Storry, C. H., Tan, J. N., Wessels, M., Grzonka, D., Oelert, W., Schepers, G., Sefzick, T., Walz, J., Pittner, H., Hänsch, T. W. & Hessels, E. A. 2002 Background-free observation of cold antihydrogen with field-ionization analysis of its states. *Phys. Rev. Lett.* **89**, 213401.

Herfurth, F., Blaum, K., Eliseev, S., Kester, O., Kluge, H.-J., Koszudowski, S., Kozhuharov, C., Maero, G., Neidherr, D., Quint, W., Schwarz, S., Stahl, S. & Vorobjev, G. 2006 The HITRAP project at GSI: trapping and cooling of highly-charged ions in a Penning trap. *Hyperfine Interact.* **173**, 93–101.

https://doi.org/10.1017/S0022377815000677 Published online by Cambridge University Press

HUANG, X.-P., ANDEREGG, F., HOLLMANN, E. M., DRISCOLL, C. F. & O'NEIL, T. M. 1997 Steady-state confinement of non-neutral plasmas by rotating electric fields. *Phys. Rev. Lett.* **78**, 875–878.

KABANTSEV, A. A., CHIM, C. Y., O'NEIL, T. M. & DRISCOLL, C. F. 2014 Diocotron and Kelvin mode damping from a flux through the critical layer. *Phys. Rev. Lett.* **112**, 115003.

KABANTSEV, A. A. & DRISCOLL, C. F. 2004 Fast measurement of picoamp plasma flows using trapped electron clouds. *Rev. Sci. Instrum.* **75**, 3628–3630.

LEPRETI, F., ROMÉ, M., MAERO, G., PAROLI, B., POZZOLI, R. & CARBONE, V. 2013 Scaling properties and intermittency of two-dimensional turbulence in pure electron plasmas. *Phys. Rev.* E **87**, 063110.

LICHTENBERG, A. J. & LIEBERMAN, M. A. 1983 *Regular and Stochastic Motion*. Springer.

LIEBERMAN, M. A. & GODYAK, V. A. 1998 From Fermi acceleration to collisionless discharge heating. *IEEE Trans. Plasma Sci.* **26**, 955–986.

MAERO, G., HERFURTH, F., KLUGE, H.-J., SCHWARZ, S. & ZWICKNAGEL, G. 2012 Numerical investigations on resistive cooling of trapped highly charged ions. *Appl. Phys.* B **18**, 1087–1096.

MAERO, G., PAROLI, B., POZZOLI, R. & ROMÉ, M. 2011 Stabilizing effect of a nonresonant radio frequency drive on the m=1 diocotron instability. *Eur. Phys. J.* D **18**, 032101.

MAERO, G., ROMÉ, M., LEPRETI, F. & CAVENAGO, M. 2014 Numerical study of a dust-contaminated electron plasma. *Eur. Phys. J.* D **68**, 1–11.

MAGGIORE, M., CAVENAGO, M., COMUNIAN, M., CHIRULOTTO, F., GALATÀ, A., DE LAZZARI, M., PORCELLATO, A. M., RONCOLATO, C., STARK, S., CARUSO, A., LONGHITANO, A., CAVALIERE, F., MAERO, G., PAROLI, B., POZZOLI, R. & ROMÉ, M. 2014 Plasma-beam traps and radiofrequency quadrupole beam coolers. *Rev. Sci. Instrum.* **85**, 02B909.

MALMBERG, J. H. & DEGRASSIE, J. S. 1975 Properties of nonneutral plasma. *Phys. Rev. Lett.* **35**, 577–580.

PAROLI, B., BETTEGA, G., MAERO, G., ROMÉ, M., NORGIA, M., PESATORI, A. & SVELTO, C. 2010*a* Electrostatic diagnostics of nanosecond pulsed electron beams in a Malmberg–Penning trap. *Rev. Sci. Instrum.* **81**, 063503.

PAROLI, B., CAVALIERE, F., CAVENAGO, M., DE LUCA, F., IKRAM, M., MAERO, G., MARINI, C., POZZOLI, R. & ROMÉ, M. 2012 Thomson backscattering diagnostic set-up for the study of nanosecond electron bunches in high space-charge regime. *J. Inst.* **7**, P01008.

PAROLI, B., DE LUCA, F., MAERO, G., POZZOLI, R. & ROMÉ, M. 2010*b* Broadband radio frequency plasma generation in a Penning–Malmberg trap. *Plasma Sources Sci. Technol.* **19**, 045013.

PAROLI, B., MAERO, G., POZZOLI, R. & ROMÉ, M. 2014 Diocotron modulation in an electron plasma through continuous radio-frequency excitation. *Phys. Plasmas* **21**, 122102.

PIERCE, J. R. 1949 *Theory and Design of Electron Beams*. D. Van Nostrand.

ROMÉ, M., CHEN, S., MAERO, G., PAROLI, B. & POZZOLI, R. 2015 Trapped electron plasma formation and equilibrium with a low-power radio-frequency drive. In *Non-Neutral Plasma Physics IX: 11th International Workshop on Non-Neutral Plasmas, AIP Conf. Proc.* (accepted for publication).

ROMÉ, M. & LEPRETI, F. 2011 Turbulence and coherent structures in non-neutral plasmas. *Eur. Phys. J. Plus* **126**, 1–17.

SAITOH, H., PEDERSEN, T. S., HERGENHAHN, U., STENSON, E. V., PASCHKOWSKI, N. & HUGENSCHMIDT, C. 2014 Recent status of a positron-electron experiment (APEX). In *13th International Workshop on Slow Positron Beam Techniques and Applications (SLOPOS13)*, Journal of Physics Conference Series, vol. 505, p. 012045. IOP Publishing.

WANG, Z., LICHTENBERG, J. & COHEN, R. H. 2012 Kinetic theory of stochastically heated RF capacitive discharges. *IEEE Trans. Plasma Sci.* **26**, 59–68.

https://doi.org/10.1017/S0022377815000677 Published online by Cambridge University Press